Experimental verification of hydrodynamic similarity in hot flows

A. J. Torregrosa[a], A. Broatch[a], J. García-Tíscar[a,*], F. Roig[a]

[a]*CMT – Motores Térmicos, Universitat Politècnica de València, Camino de Vera, 46022 Valencia, Spain*

Abstract

This paper examines a common hypothesis in the design of internal combustion engine exhaust lines, namely that the ratio of the total pressure drop across the line to the inlet dynamic head should be a function only of the Reynolds number. While incompressible flow theory, provided that some simplifications are considered, is often used in support of this hypothesis, detailed experimental verification in actual exhaust lines is absent from the literature. Production exhaust lines contain non-trivial flow complexities such as muffler devices and catalytic converters and, in the case of high-performance engines, often operate at high temperature and high mass flow conditions, thereby rendering the usual theoretical simplifications doubtful. In this work, a production exhaust line composed of cold and hot ends, featuring a muffler and a catalytic converter, is tested at a variety of conditions. Analysis of the results shows that compressibility corrections must be factored in at certain conditions routinely found in actual high-performance engines, and that for hot ends, laminar flow at the converter monolith channels may pose a challenge to the hydrodynamic similarity hypothesis.

Keywords: *Automotive engineering, Exhaust lines, Catalytic converters, Internal combustion engines*

1. Introduction

Backpressure is, together with acoustic attenuation and flow noise generation, one of the main aspects defining the design of exhaust lines for internal combustion engines [1–4]. Processes affecting cylinder discharge are, in principle, highly unsteady, as the main role is played by the instantaneous pressure downstream of the exhaust valves, that is the result of complex wave-dynamics interactions between the different cylinders and the acoustics of the exhaust line. However, it has been demonstrated [5] that for medium to high engine speeds the fluctuations associated with unsteady motion are significantly smaller than the mean value of the flow velocity. Under these conditions, pressure fluctuations are also small, and the flow may be regarded as a steady flow with a superimposed perturbation. Of course this also applies to the pressure downstream of the valves, so that backpressure may be estimated with sufficient precision by determining the steady pressure drop across the exhaust line, which is a convenient simplification of the problem [6, 7].

Once this assumption is accepted, according to incompressible flow theory the ratio of the total (stagnation) pressure drop across the system to the inlet dynamic head should be a function only of the Reynolds number [8, 9]. Given all the simplifications assumed in order to reach this point, it is reasonable to put the question if this is actually the case, even if high temperatures and high mass flows as those present in the exhaust of high-displacement, high-performance engines are considered.

The purpose of the present work is providing an answer to such question, as it appears that a direct experimental assessment is missing in the literature. With that objective, pressure drop measurements were taken on different exhaust systems (both hot and cold ends) at different mass flows and inlet temperatures. The results were then analyzed in the context of incompressible flow theory, showing the limitations of such approach. Consideration of compressible flow effects, however, indicate that hydrodynamic similarity essentially holds in all the conditions considered, and thus cold-flow measurements may be sufficiently indicative and suitable for sound extrapolation to real engine exhaust conditions.

2. Methodology

In this section, the measurements are briefly described and the theoretical analysis supporting data reduction and processing is described in detail.

2.1. Exhaust system

The complete exhaust system considered in this investigation is from actual production models, representative of current designs, and is composed of a cold end and a hot end. The former includes a single rear muffler and the corresponding ducting, whereas the latter comprises a catalytic converter and again, its corresponding ducting. Figure 1 illustrates the design of both hot and cold ends.

Measurements were performed separately for the cold and hot ends, in order to assess the differences in the flow behaviour between both of them.

*Corresponding author. Email address: jorgarti@mot.upv.es

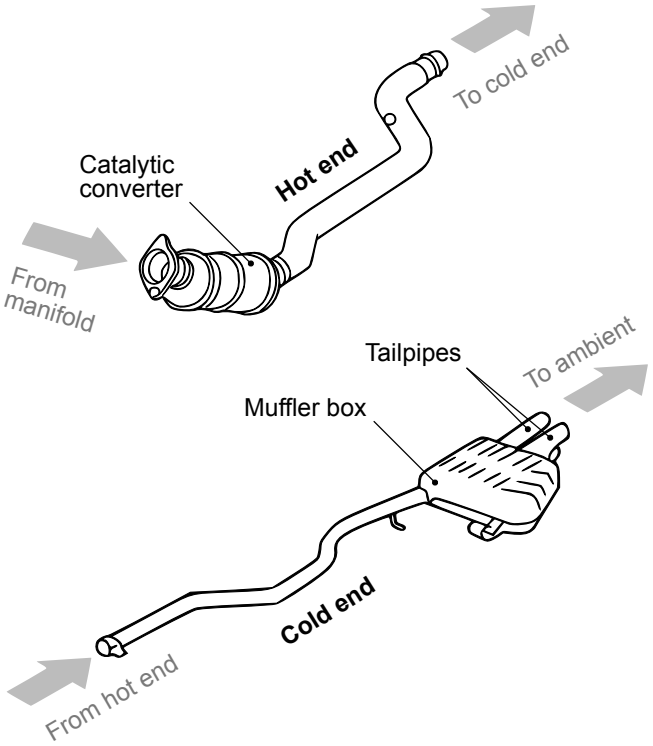

Figure 1: *Sketches of the hot (top) and cold (bottom) ends characterized in this investigation (drawing not to scale).*

2.2. Experimental facilities

Experiments on both cold and hot ends were carried out in two different experimental setups, that are described next.

2.2.1. Conventional flow rig

The first of these experimental facilities is the Moderate Flow and Moderate Temperature (MFMT) test bench, a conventional, steady flow rig with air supplied by a roots blower and described in previous works [10]. A settling tank is included in the air circuit in order to eliminate any possible disturbance caused by the blower, and to ensure smooth, fully developed air flow with no tangential velocity. In this rig, electrical heaters were used to increase the flow temperature up to 400 ºC. Due to power limitations, the values reached for the mass flow are smaller the higher is the temperature considered.

Mass flow was measured with a hot-plate anemometer, pressure measurements were taken with water columns, that provide a very high degree of precision, and temperature readings were obtained by means of thermocouples. In the top of Figure 2 the floor plan of this facility can be seen, including the selected cold end.

2.2.2. High flow and high temperature rig

The second facility is the High Flow and High Temperature (HFHT) test bench, a singular installation powered by an industrial compressor which blows into two large settling tanks in order to provide smooth flow to the measurement room. Bleed valves are available in order to dump excess mass flow while keeping the compressor operating at a given pressure. Additional control valves of different sizes can be used as well to restrict the mass flow without dumping.

This test rig is also equipped with a combustion chamber, thus allowing higher mass flows and higher temperatures (up to 2000 kg/h and 600 ºC) than the conventional test rig. An air extractor connected to a large silencer is located in the measurement room, in order to evacuate the hot air flow. In addition, the walls of this chamber are acoustically treated, in order to isolate the rest of the building from the flow noise being generated. The floor plan of this facility can be seen in

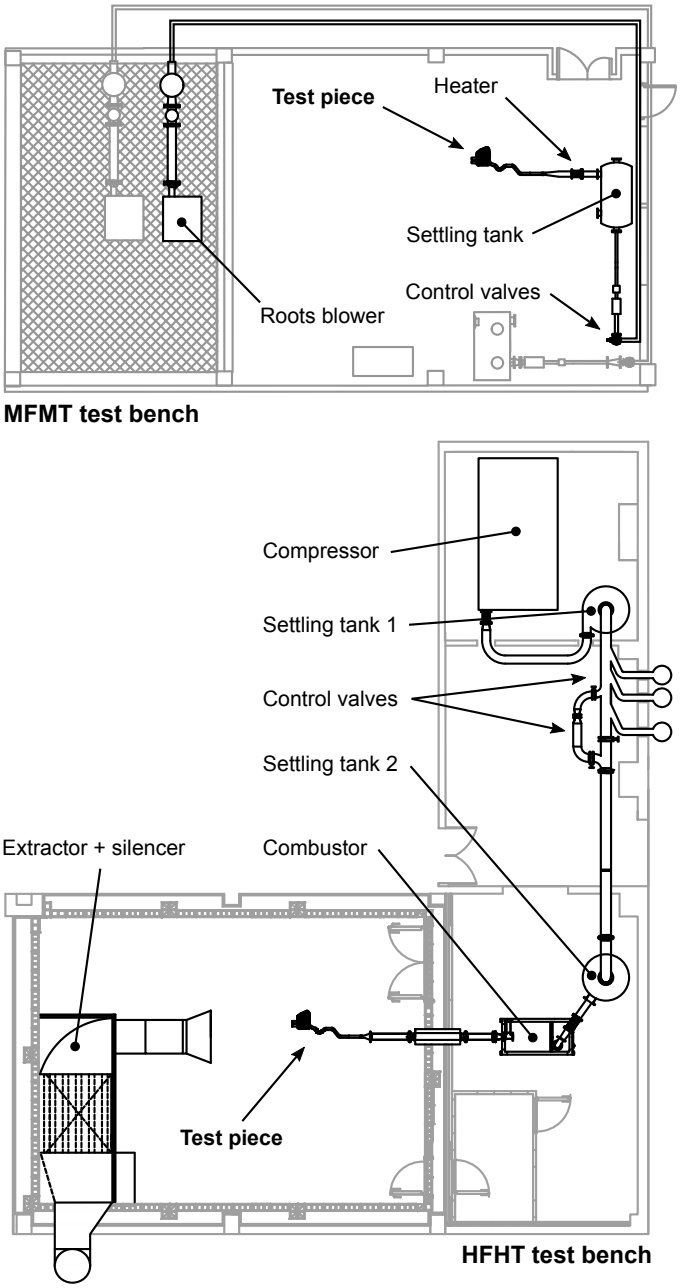

Figure 2: *Floor plans of the facilities used: MFMT test bench (top) and HFHT test bench (bottom).*

the bottom of Figure 2.

In this case, mass flow was measured with a differential pressure flow meter, whereas pressure measurements were taken with piezorresistive transducers. Again, temperature readings were obtained through the use of thermocouples.

It will be seen later on that a full compatibility was found between the results of the two experimental setups, ensuring that the observed trends in the flow behaviour were not due to the particularities of a given test rig.

2.3. Incompressible flow analysis

The pressure drop of any system carrying an incompressible flow may be written as:

$$\Delta p = K\frac{1}{2}\rho U^2 \tag{1}$$

where Δp is the pressure drop, ρ and U are respectively the inlet density and area-averaged velocity, and K is a pressure drop coefficient that, for a given system, should be a function only of the Reynolds number (Re) [8]. Of course, the fact that the pressure drop is referred to the inlet dynamic head does not necessarily imply a quadratic dependence of pressure drop on the flow velocity. Such dependence is only achieved at relatively high Reynolds numbers, when the pressure drop coefficient is essentially constant. This is in fact what defines the conditions corresponding to a fully developed turbulent flow. In any other case, the dependence of K with Re will result in a non-quadratic dependence between Δp and U.

In the case of a cold end, one may assume that if the flow is fully developed at the inlet section it will remain fully developed all along the system. It is then possible to express the pressure drop as a quadratic function of the mass flow $\dot{m}$: recalling that $\dot{m} = \rho UA$, where A is the cross-sectional area of the duct, one has:

$$\Delta p = \frac{1}{2}K\frac{1}{\rho A^2}\dot{m}^2 \tag{2}$$

Therefore, the pressure drop should depend linearly with the quantity $\dot{m}^2/\rho$, and this provides a check of the main assumption in terms mostly of measured magnitudes (pressure drop and mass flow) with only the density being indirectly determined from the equation of state and the measured values of pressure and temperature T, as $\rho = p/RT$.

In the case of a hot end, which includes a catalytic converter with its monolith, the small section of the passages in the monolith bundle should give rise to a dependence that includes, together with the quadratic term associated with turbulent losses at the inlet and the outlet of the monolith, a linear term representing the laminar pressure drop across the monolith itself [11, 12]. The total resulting pressure drop can be expressed thus as:

$$\Delta p = \frac{1}{2}K\frac{1}{\rho A^2}\dot{m}^2 + \psi\,\nu\,\dot{m} \tag{3}$$

where ψ is a term that depends only on the monolith geometry, and ν is the kinematic viscosity. It is apparent here that $\dot{m}^2/\rho$ is no longer a convenient variable for the analysis. In this case, with the same purpose as before of making use mainly of measured magnitudes, it is preferable instead to rewrite Eq. 3 as:

$$\rho\Delta p = \frac{1}{2}K\frac{1}{A^2}\dot{m}^2 + \psi\mu\,\dot{m} \tag{4}$$

where $\mu = \rho\nu$ is the dynamic viscosity, which for air is essentially a function only of temperature. The following correlation, based on Sutherland's expression [13], was used to represent this dependence:

$$\mu(T) = 1.82\cdot 10^{-5}\sqrt{\frac{T}{293}}\left(\frac{1.3891}{1+\frac{114}{T}}\right) \tag{5}$$

In this way, one should expect that, when fitting the observed values of $\rho\Delta p$ as a quadratic function of $\dot{m}$ (with no intercept) the coefficient of the quadratic term should be essentially a constant, whereas the coefficient of the linear term should exhibit a dependence on temperature consistent with the temperature dependence of the dynamic viscosity.

Equations 2 and 4 provide the basis for the analyses presented, separately for the cold and the hot ends, in the forthcoming section.

The uncertainty values for the above defined flow variables can be found in table 1. Pressure, temperature and mass flow rate uncertainties are directly measured and therefore the sensor uncertainty is used, whereas propagation of uncertainty has been computed for the rest of the variables assuming worst-case flow conditions (min. p, T and $\dot{m}$).

Table 1: *Uncertainty of the relevant variables*

Variable	Symbol	Uncertainty
Pressure	p	±0.250 %
Temperature	T	±1.000 K
Mass flow rate	$\dot{m}$	±0.500 %
Density	ρ	±0.344 %
Dynamic viscosity	μ	±0.128 %
Ratio of specific heats	γ	±0.027 %
Expansion factor	Φ	±0.974 %

3. Results analysis for a cold end

A cold end comprising a single rear muffler and the corresponding upstream and downstream ducting was considered. Measurements were taken in the two experimental setups indicated in section 2.2 and, in order to provide an overall view of the scope of the results obtained, the relation between the Reynolds number and the Mach number corresponding to all the operating conditions considered is plotted in Figure 3.

It is apparent that, as indicated above, the results obtained from the two rigs are fully consistent, since the same trends are observed in the curves corresponding to the same flow temperature. It is also apparent that the Reynolds numbers

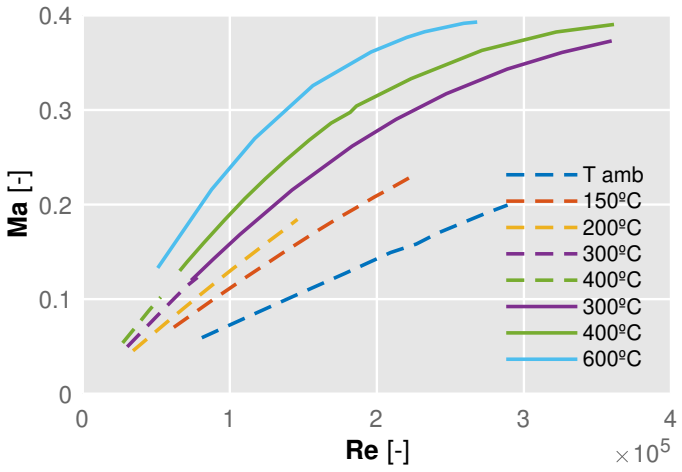

Figure 3: *All operating points of the cold end represented on a Re vs. Ma plot. Dashed lines were measured in the MFMT test bench and solid lines were measured in the HFHT test bench.*

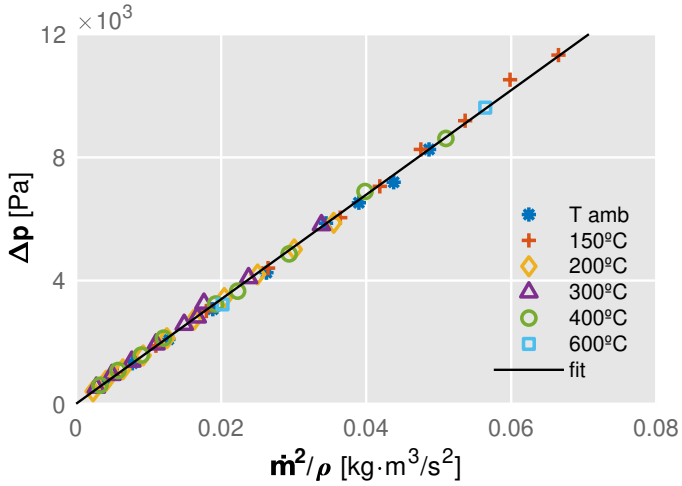

Figure 4: *Representation of Δp in the cold end measurements as a function of $\dot{m}^2/\rho$ for Ma < 0.2.*

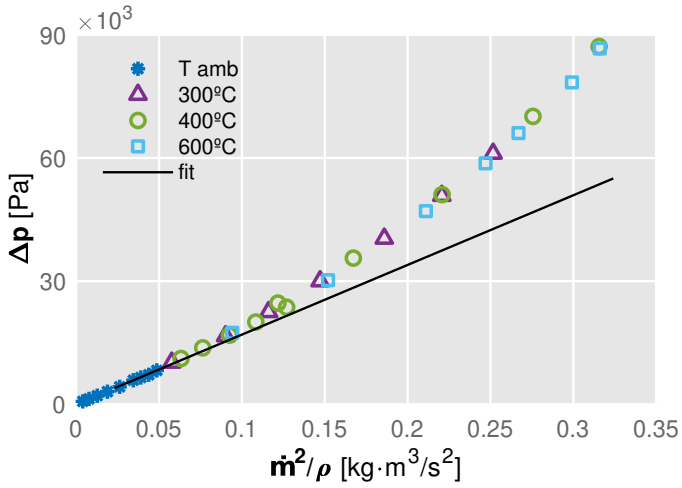

Figure 5: *Representation of Δp in the cold end measurements as a function of $\dot{m}^2/\rho$ for Ma > 0.2.*

achieved are sufficiently high so as to assume that in virtually all the cases the flow is a fully developed turbulent flow.

However, it can also be noticed that relatively high values of the Mach number are achieved (close to 0.4 at the highest temperature of 600ºC), while it is usually considered that flows may be soundly considered as incompressible for Mach numbers below 0.2. Therefore, some deviations from the expected behaviour may be found, and the quantification of such deviations may turn out to provide relevant information on the applicability of the usual practice, as the conditions considered are realistic, the steady character of the flow being the only major assumption.

Therefore, the analysis was performed separately for those cases in which Ma < 0.2 (thus allowing for a fully incompressible description) and those in which Ma > 0.2 and one may expect some effects of compressibility, irrespective of the rig used to perform the test. Results of representing Eq. 2 in the incompressible cases are shown in Figure 4.

The representation exhibits a clearly linear dependence of Δp on $\dot{m}^2/\rho$ and a satisfactory collapse of the values obtained at different temperatures. One may therefore conclude that, in these conditions, the flow similarity holds within the experimental uncertainties, so that any dependence on temperature is related with the associated change in density, and the pressure drop coefficient is essentially a constant.

The results obtained for the same representation in the cases where Ma > 0.2 are shown in Figure 5, together with the fit obtained in the incompressible cases. It is now apparent that a significant deviation exists between the measured pressure drop and that expected according to an incompressible flow analysis. It is also apparent that the deviation observed exhibits a well-defined and consistent trend that, in principle, could only be due to compressible flow effects.

Actually, the behaviour observed corresponds to the well-known fact that, in compressible flow, the mass flow associated with a given pressure drop is smaller than its incompressible counterpart. This effect is usually taken into account (for instance, in flow metering applications) by the inclusion in Eq. 2 of an expansion factor Φ so that

$$\dot{m} \propto \Phi \sqrt{\rho \Delta p} \tag{6}$$

Considering this, Eq. 2 can be rewritten as

$$\Phi^2 \Delta p = \frac{1}{2} K \frac{1}{\rho A^2} \dot{m}^2 \tag{7}$$

and therefore similarity would imply a linear dependence of $\Phi^2 \Delta p$ on $\dot{m}^2/\rho$. A usually accepted empirical expression for the expansion factor Φ in flow metering applications [14, 15] is

$$\Phi = 1 - \frac{1.4}{\xi \gamma} \frac{\Delta p}{p} \left[1 - \left(\frac{2}{\gamma + 1} \right)^{\frac{\gamma}{\gamma - 1}} \right]^{-1} \tag{8}$$

where ξ is a sort of calibration factor dependent on the particular system, and γ is the ratio of specific heats, whose

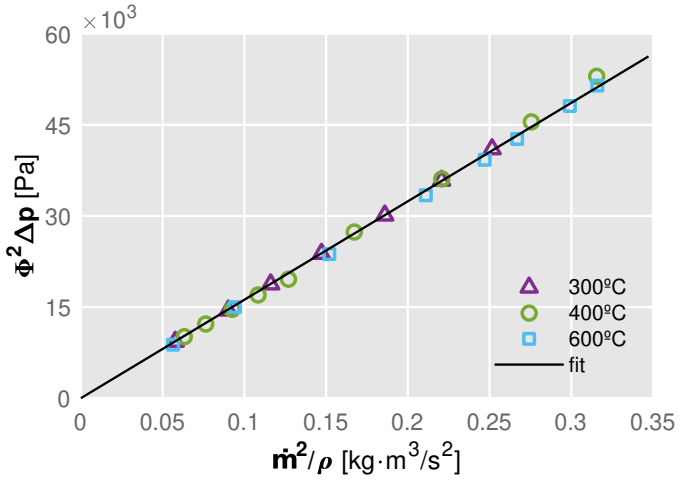

Figure 6: *Representation of $\Phi^2\Delta p$ in the cold end measurements as a function of $\dot{m}^2/\rho$ for Ma > 0.2.*

dependence with temperature has been described with the following correlation: [16]

$$\gamma(T) = 1.35193 + T(4.246\times10^{-4} + T(-1.196\times10^{-6} + T(1.186\times10^{-9} - 4.38\times10^{-13}T))) \quad (9)$$

The dependence of $\Phi^2\Delta p$ on $\dot{m}^2/\rho$ for the compressible cases is plotted in Figure 6. The value of the system dependent constant ξ was set to 4.5 for the best agreement, which was considered reasonable as it is of the same order of magnitude as the standard value $\xi = 3$ suggested for a simple restriction.

It is apparent that the collapse achieved is comparable to that observed in Figure 4 for the incompressible cases. One may therefore conclude that, also in these conditions, the flow similarity holds within the experimental uncertainties, once compressibility is accounted for.

4. Results analysis for a hot end

A hot end comprising a single catalytic converter and the corresponding upstream and downstream ducting was considered. Again, measurements were taken in the two experimental setups indicated in section 2.2 and the relation between the Reynolds number and the Mach number corresponding to all the operating conditions was analyzed.

The corresponding representation is given in Figure 7, where again the consistency of the results obtained from the two rigs is apparent. The Reynolds numbers achieved are sufficiently high so as to assume that in virtually all the cases the inlet flow is a fully developed turbulent flow. However, inside the monolith channels the flow is expected to be locally laminar.

Regarding the Mach number, the values obtained are somehow smaller than those of the cold end, but are still relatively high (close to 0.33 at the highest temperature of 600ºC), and it is thus expected that some deviations from the incompressible behaviour represented by Eq. 4 may be found.

Therefore, in the same way as for the cold end the results were analyzed separately for those cases with Ma < 0.2 (incompressible flow) and those with Ma > 0.2 (compressible flow), using together when possible the results from the two setups. Results of representing Eq. 4 in the incompressible cases are shown in Figure 8.

It can be observed that $\rho\Delta p$ can be fairly fitted to a dependence on the mass flow for each temperature that includes a quadratic and a linear term with no intercept, as indicated by Eq. 4. However, there is still a residual dependence on temperature, that should be attributed to the linear contribution.

In order to verify this, one should check if the dependence with temperature of the linear coefficient of the fits is essentially related with the dependence of dynamic viscosity, and the factor ψ is solely related with the geometry of the device (more precisely, with the ratio of the chamber area to the total effective area of the monolith).

This check is provided in Figure 9, where it can be observed that the coefficient exhibits the correct tendency, even if a considerable scatter is apparent. Of course, the determination of the coefficients themselves is affected by the fitting error. However, this information was used in order to estimate, even if approximately, the contribution of the linear term and, as a consequence, to check the behaviour of the quadratic term alone.

Therefore, an approximate evaluation of the quadratic dependence was obtained by analyzing the quantity

$$\rho\Delta p - \psi\mu\dot{m} = \frac{1}{2}K\frac{1}{A^2}\dot{m}^2 \quad (10)$$

where ψ is obtained by fitting the linear cofficents of the quadratic regressions shown in Figure 8 to a linear regression without intercept, as shown in Figure 9. The corresponding results are then plotted in Figure 10.

Given all the approximations involved, the collapse achieved may be regarded as satisfactory, even if the scatter is larger than that obtained in the case of the cold end.

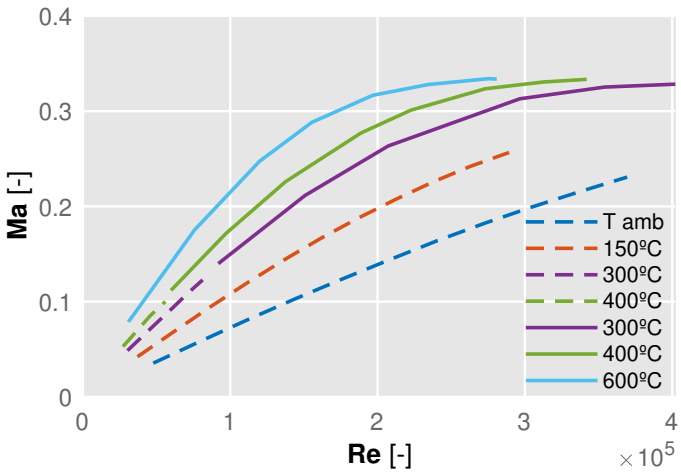

Figure 7: *All operating point of the hot end represented on a Re vs. Ma plot. Dashed lines were measured in the MFMT test bench and solid lines were measured in the HFHT test bench.*

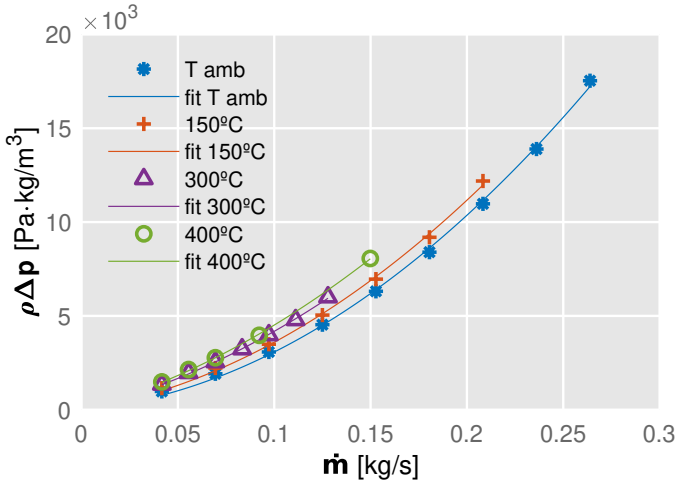

Figure 8: *Representation of $\rho\Delta p$ in the hot end measurements as a function of $\dot{m}$ for Ma < 0.2, along with quadratic fits for each temperature condition.*

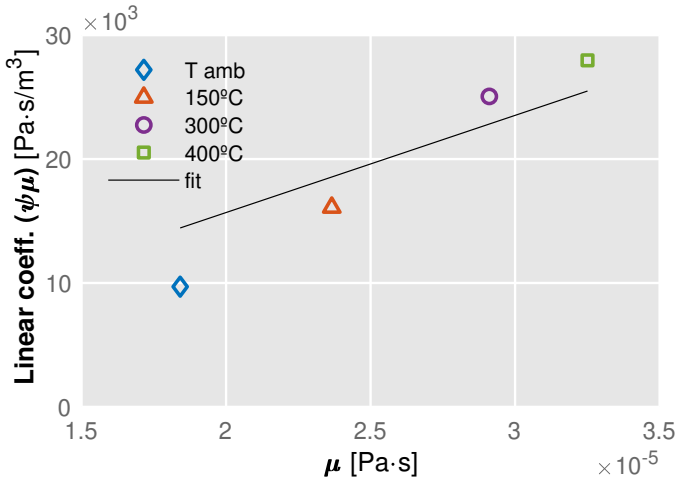

Figure 9: *Linear coefficients $(\psi\mu)$ of the fits shown in Figure 8 as a function of μ. The slope of the linear fit is therefore ψ.*

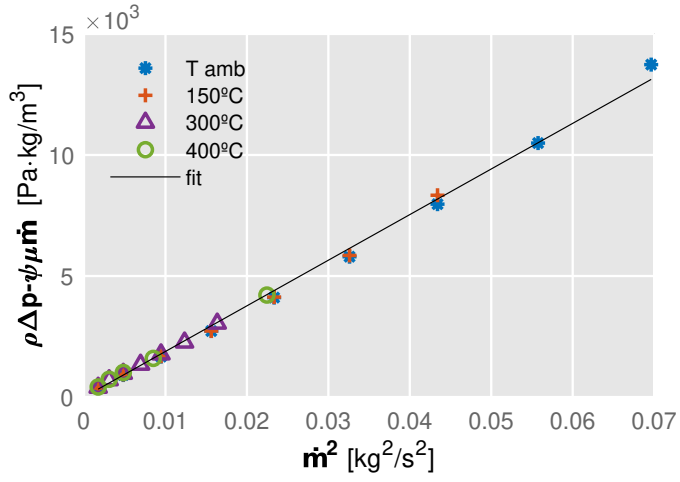

Figure 10: *Representation of $(\rho\Delta p - \psi\mu\dot{m})$ in the hot end measurements as a function of $\dot{m}^2$ for Ma < 0.2.*

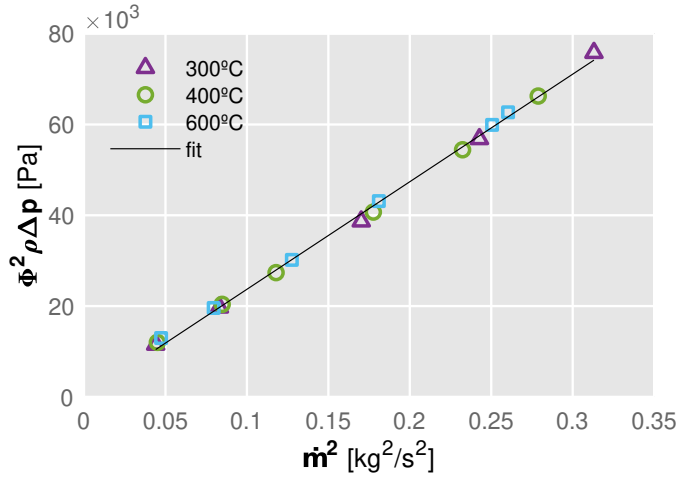

Figure 11: *Representation of $\Phi^2\rho\Delta p$ in the hot end measurements as a function of $\dot{m}^2$ for Ma > 0.2.*

Therefore, one may conclude that, also in this case, if the flow may be regarded as incompressible the similarity holds at least to a degree that provides sufficient confidence for its application in practical problems of exhaust design.

For the compressible flow case however, an analysis of $\Phi^2\rho\Delta p$ versus $\dot{m}^2$, this is, the same approach performed earlier in the compressible flow case for the cold end, results in a good linear fitting, as seen in Figure 11. Here, the value of ξ has been kept at 4.5 as in the aforementioned case.

In view of the results of Figure 11, it seems that for the compressible flow case in the hot end, the hydrodynamic similarity hypothesis can be used without taking into account the linear terms, as in the incompressible flow case, once that the Φ factor is used to account for compressibility. In fact, as shown in Figure 12, the linear correction may be dropped entirely, and still an overall quadratic K factor collapses the pressure loss data.

If following Eq. 3 the quadratic pressure drop factor K is assigned to the contraction and expansion losses [12] and the linear factor ψ to the friction losses along the monolith channels, it therefore follows that in compressible flow conditions the latter scale with $\dot{m}$ much less than the former.

It might also be possible that the oblique pressure loss K_α discussed by Persoons et al. [11, 12] becomes dominant at these regimes, since at higher Mach numbers the flow may lose its ability to properly develop before entering the monolith channels, leading to an increase in tangential velocity that is correlated with the oblique pressure loss term, that also scales with $\dot{m}^2$. However, determining if this is the case would require a detailed flow analysis taking into account the actual 3D geometry of the hot end, which is beyond the scope of the 0D analysis carried out in this investigation.

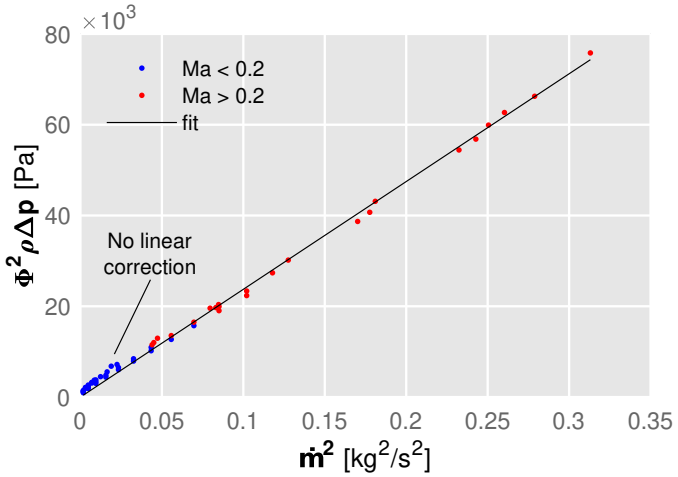

Figure 12: *Representation of $\Phi^2 \rho \Delta p$ in the hot end measurements as a function of $\dot{m}^2$ for all Ma values.*

5. Summary and conclusions

From the work presented here, the following conclusions can be extracted:

- In the conditions considered (up to 2000 kg/h and 600ºC) both incompressible and compressible aspects may be relevant.
- At any given temperature, the overall evolution of pressure drop with mass flow is as expected, for both cold and hot ends (in the last case, including a significant laminar contribution).
- In cold ends, the observed dependence with temperature is consistent with an essentially constant pressure drop coefficient, once compressibility effects are included when pertinent.
- In hot ends, the complexity induced by the laminar term makes the results less convincing, but it seems legitimate to conclude that:
  - For incompressible flow, hydrodynamic similarity is also verified, even if approximately, when introducing a linear correction term.
  - For compressible flow the quadratic pressure losses are dominant, and the hydrodynamic similarity may hold provided a suitable compressibility factor is used.

Acknowledgements

The equipment used in this work has been partially supported by FEDER project funds “Dotación de infraestructuras científico técnicas para el Centro Integral de Mejora Energética y Medioambiental de Sistemas de Transporte (CiMeT), [FEDER-ICTS-2012-06]” framed in the operational program of unique scientific and technical infrastructure of the Spanish Ministerio de Economía y Competitividad.

F. Roig is supported through the Programa de Apoyo para la Investigación y Desarrollo of the Universitat Politècnica de València [PAID-01-17].

The authors wish to thank L. Smith and G. Lingannaiah for the inspiration to write the paper, and A. Guzmán for his invaluable assistance in the measurements.

References

[1] D. Rowley, Exhaust system considerations for 1982 heavy duty trucks, in: SAE Technical Paper, SAE International, 1977. doi:10.4271/770893.

[2] D. Deshmukh, J. Modak, K. Nayak, Experimental analysis of backpressure phenomenon consideration for c.i. engine performance improvement, in: SAE Technical Paper, no. 2010-01-1575, SAE International, 2010. doi:10.4271/2010-01-1575.

[3] N. Kumar, A. Saroop, A. Kuchhal, V. Chauhan, S. Sharma, Effect of muffler characteristics on performance of a naturally aspirated si engine, in: SAE Technical Paper, no. 2013-01-2834, SAE International, 2013. doi:10.4271/2013-01-2834.

[4] T. George, H. Raj, Energy efficient design and modification of an automotive exhaust muffler for optimum noise, transmission loss, insertion loss and back pressure: A review, International Conference on Mechanical, Materials and Renew. Energ.doi:10.1088/1757-899X/377/1/012127.

[5] A. Torregrosa, A. Broatch, V. Bermudez, I. Andres, Experimental assessment of emission models used for ic engine exhaust noise prediction, Exp. Therm. Fluid Sci. 30 (2) (2005) 97–107. doi:10.1016/j.expthermflusci.2005.05.001.

[6] J. Kim, M. Corsetti, L. Biundo, D. Dobson, R. Beason, Modeling and measuring exhaust backpressure resulting from flow restriction through an aftertreatment system, in: SAE Technical Paper, no. 2003-01-0939, SAE International, 2003. doi:10.4271/2003-01-0939.

[7] M. Dixit, V. Sundaram, S. Kumar, A novel approach for flow simulation and back pressure prediction of cold end exhaust system, in: SAE Technical Paper, no. 2016-28-0235, SAE International, 2016. doi:10.4271/2016-28-0235.

[8] D. Miller, Internal Flow Systems, BHRA Fluid Engineering series, BHRA (Information Services), 1990.
URL https://books.google.es/books?id=8pJRAAAAMAAJ

[9] D. Ukrop, M. Shanks, M. Carter, Predicting running vehicle exhaust back pressure in a laboratory using air flowing at room temperature and spreadsheet calculations, in: SAE Technical Paper, no. 2009-01-1154, SAE International, 2009. doi:10.4271/2009-01-1154.

[10] F. Payri, A. Torregrosa, A. Broatch, J. Brunel, Pressure loss characterisation of perforated ducts, in: SAE Technical Paper, no. 980282, SAE International, 1998. doi:10.4271/980282.
URL https://doi.org/10.4271/980282

[11] T. Persoons, M. Vanierschot, E. Van den Bulck, Stereoscopic piv measurements of swirling flow entering a catalyst substrate, Exp. Therm. Fluid Sci. 32 (8) (2008) 1590–1596. doi:10.1016/j.expthermflusci.2008.04.011.

[12] T. Persoons, M. Vanierschot, E. Van den Bulck, Oblique inlet pressure loss for swirling flow entering a catalyst substrate, Exp. Therm. Fluid Sci. 32 (6) (2008) 1222–1231. doi:10.1016/j.expthermflusci.2008.02.002.

[13] W. Sutherland, The viscosity of gases and molecular force, The London, Edinburgh, and Dublin Philosophical Magazine and Journal of Science 36 (223) (1893) 507–531. doi:10.1080/14786449308620508.

[14] Crane Company. Engineering Division, Flow of fluids through valves, fittings, and pipe, Tech. Rep. TP-410 (1942).

[15] Fisher, Control valve handbook, 4th Edition, Emerson Process Management, Marshalltown, Iowa 50158 USA, 2005.

[16] J. Keenan, J. Chao, J.Kaye, Gas tables. Thermodynamic properties of air products of combustion and component gases compressible flow functions, John Wiley and Sons, 1983. doi:10.1021/ed059pA70.1.